Modeling and Multivariable Control of a Novel Multi-Dimensional Levitated Stage with High Precision

Tiejun Hu and Won-jong Kim*

Abstract: This paper presents the modeling and multivariable feedback control of a novel high-precision multi-dimensional positioning stage. This integrated 6-degree-of-freedom (DOF) motion stage is levitated by three aerostatic bearings and actuated by 3 three-phase synchronous permanent-magnet planar motors (SPMPMs). It can generate all 6-DOF motions with only a single moving part. With the DQ decomposition theory, this positioning stage is modeled as a multi-input multi-output (MIMO) electromechanical system with six inputs (currents) and six outputs (displacements). To achieve high-precision positioning capability, discrete-time integrator-augmented linear-quadratic-regulator (LQR) and reduced-order linear-quadratic-Gaussian (LQG) control methodologies are applied. Digital multivariable controllers are designed and implemented on the positioning system, and experimental results are also presented in this paper to demonstrate the stage's dynamic performance.

Keywords: Integrator-augmented LQR, reduced-order LQG, precision motion control, synchronous permanent-magnet planar motor, multivariable control.

1. INTRODUCTION

In the semiconductor manufacturing industry, the number of transistors that can be placed on an integrated circuit (IC) doubles every couple of years or so according to Moore's law [1]. Especially with the ever-increasing demands for higher-storage-density memory chips from the high-tech market all around the world, the 193-nm lithography is now fully employed in chip manufacturing [2]. In the high-accuracy positioning and sophisticated lithographic process, wafer steppers are used to manufacture ICs via fully automated control [3]. Higher-precision wafer steppers, along with other strategic manufacturing equipment, must be available at least two years before the production ramps up.

Conventional high-precision positioning stages usually have cumbersome stacked structures. They are in either crossed-axis-type or gantry-type configuration with mechanical gear, ball- or lead-screw drives [4]. Manufacturing accuracy requirements for the mechanical parts of these conventional stages are extremely demanding. Piezoelectric (PZT) actuators are another type of high-precision positioning devices [5,6]. They can easily achieve a sub-micrometer positioning resolution. However, a PZT-actuated stage has very limited travel range (usually on the order of micrometers to tens of micrometers [7]).

Compared with these conventional high-precision positioning devices, multi-dimensional stages actuated by planar motors possess potential advantages such as high accuracy, ease in driving, no backlash, low friction, and so on. By their working principles, most of the planar motors can be classified into three types: Sawyer motors, SPMPMs, and induction planar motors [8]. Among them, the induction planar motors are still in their development stage [9]. Sawyer motors can offer fairly high precision but are susceptible to loss of steps and unable to provide high stiffness [10]. Moreover, as their motion is tightly constrained to a plane, a Sawyer motor could not provide focus range or local leveling without using other fine motion actuators.

The multi-dimensional positioning stage presented in this paper is actuated by 3 three-phase SPMPMs attached on the bottom surface of the single moving part, namely the platen. It can generate all required fine and coarse motions with only one levitated moving part. Fig. 1 shows a photograph of the constructed multi-dimensional positioning stage. The concentrated-field permanent-magnet matrix beneath the aluminum sheet is made by superimposing two Halbach magnet arrays [11,12]. By changing the

Manuscript received May 24, 2005; revised September 9 2005; accepted October 7, 2005. Recommended by Editor Keum-Shik Hong. This work was in part based upon work supported by the Texas Advanced Technology Program under Grant No. 000512-0225-2001.

Tiejun Hu was with the Department of Mechanical Engineering, Texas A&M University, College Station, TX 77843, U.S.A. (e-mail: hu_tie_jun@hotmail.com).

Won-jong Kim is with the Department of Mechanical Engineering, Texas A&M University, College Station, TX 77843, U.S.A. (e-mail: wjkim@tamu.edu).

* Corresponding author.

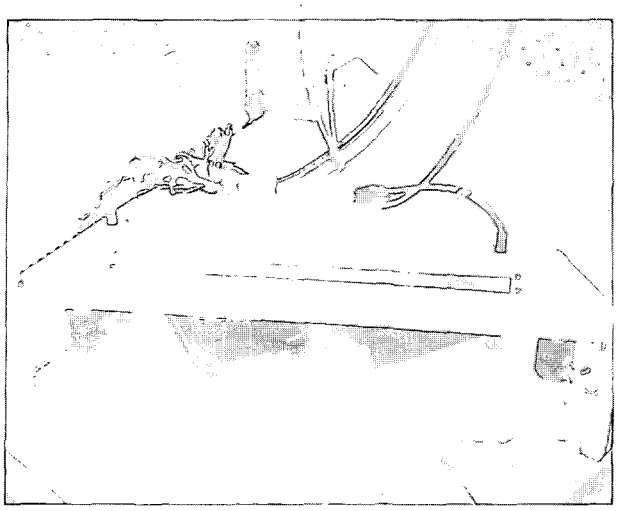

Fig. 1. A photograph of the multi-dimensional stage. The triangular platen is placed on top of a mirror-finished aluminum sheet. Beneath the aluminum sheet is the concentrated-field permanent magnet matrix [11].

magnitude and direction of their phase currents, the three SPMPMs generate both levitation and driving forces. The detailed working principle including the electromagnetic analysis has already been fully illustrated in our previous publication [13].

This multi-dimensional positioning stage is levitated by three aerostatic bearings. Thus there is no mechanical friction between the moving part and the stationary machine frame. Therefore, it will not generate any wear particles and is clean-room compatible. Furthermore, this multi-dimensional positioning stage can provide a unique combination of long travel range and high positioning resolution that can be achieved by applying advanced multivariable control algorithm.

In this paper, the dynamic analysis, system modeling, and multivariable controller design will be discussed. A model describing the dynamic behavior of the multidimensional positioning stage is developed in the next section [14]. Experimental results are also presented to demonstrate the effectiveness of the designed MIMO controllers. Conclusions on the experimental results and performances of different multivariable controllers are given at the end this paper.

2. MODELING

In this section, the dynamics of the multi-dimensional positioning stage is first analyzed. Then the corresponding state-space model of the system will be derived. Fig. 2 illustrates our convention for the coordinate system and the directions of the 6 independent force components generated by the three SPMPMs.

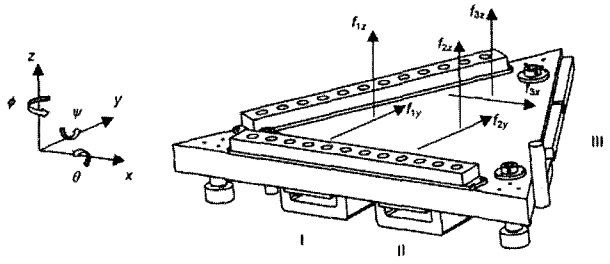

Fig. 2. Coordinate system and force convention of the multi-dimensional positioning stage.

Table 1. 6-DOF motion generation by the SPMPMs.

	Motor I	Motor II	Motor III
x	0	0	f_{3x}
y	f_{1y}	f_{2y}	0
z	f_{1z}	f_{2z}	f_{3z}
θ	$-f_{1z}$	$-f_{2z}$	f_{3z}
ψ	f_{1z}	$-f_{2z}$	0
φ	$-f_{1y}$	f_{2y}	0

The windings of the 3 three-phase SPMPMs I, II, and III are attached on the bottom surface of the platen (as shown in Fig. 2). Motors I and II are responsible for generating magnetic forces f_{1y} and f_{2y} in the y-direction. Motor III can generate the x-direction force f_{3x}. All the three motors I, II, and III can generate z-direction forces f_{1z}, f_{2z}, and f_{3z} individually [12]. By changing the magnitude and direction of the magnetic forces generated by these three planar motors, the controller can make the stage generate translations in the x-, y-, and z-directions as well as rotational motions around these axes. The detailed method used to generate motions in all six axes is presented in Table 1.

The relation between the electrical subsystem and the mechanical subsystem is linked by the magnetic force equation (1), which is derived by the electromagnetic analysis [12,15].

$$\begin{bmatrix} f_y \\ f_z \end{bmatrix} = \frac{1}{2}\mu_0 M_0 \eta_0 N_m G e^{-\gamma_1 z_0} \begin{bmatrix} \cos\gamma_1 y & \sin\gamma_1 y \\ -\sin\gamma_1 y & \cos\gamma_1 y \end{bmatrix} \begin{bmatrix} \frac{2}{3} & -\frac{1}{3} & -\frac{1}{3} \\ 0 & \frac{1}{\sqrt{3}} & -\frac{1}{\sqrt{3}} \end{bmatrix} \begin{bmatrix} i_A \\ i_B \\ i_C \end{bmatrix} \tag{1}$$

where f_y and f_z are the y-directed and z-directed forces, respectively, and i_A, i_B, and i_C are the input phase currents (each planar motor has three phases). The constant

$$G = \frac{\sqrt{2}wl^2}{\pi^2}\left(1 - e^{-\gamma_1 \Gamma}\right)\left(1 - e^{-\gamma_1 \Delta}\right) \tag{2}$$

contains the effects of the motor geometry and is 1.072×10^{-5} m^3. The variable y represents a relative displacement in motors I and II. The parameters have

the following values: magnet remanence, $\mu_0 M_0 = 0.71$ T, effective spatial period $N_m = 2$, pitch $l = 50.98$ mm, absolute value of the fundamental wave number $\gamma_1 = 2\pi/l = 123.25$ m^{-1}, the nominal motor air gap $z_0 = 2.32$ mm, the magnet array thickness, $\Delta = l/4 = 12.70$ mm, and the winding thickness, $\Gamma = l/5 = 10.16$ mm. Equation (1) presents only the force component for one planar motor in the y-direction. Motor III has a similar force equation in f_x and f_z with the corresponding displacement variable x due to the symmetry of the concentrated-field magnet matrix.

Three laser interferometers with a resolution of 0.6 nm and three laser distance sensors with a resolution of 15 nm are used to measure the horizontal and vertical position of the stage. Since the stage is levitated by air bearings, there is no mechanical friction between the stage and the base plate. Thus, the dynamics of the stage in the horizontal mode can be represented with a pure-mass model as follows.

$$m\frac{d^2x}{dt^2} = f_x \tag{3}$$

$$m\frac{d^2y}{dt^2} = f_y \tag{4}$$

$$I_{zz}\frac{d^2\varphi}{dt^2} = \tau, \tag{5}$$

where m is the mass of the platen, which is 5.91 kg, and f_x and f_y are the magnetic forces generated by the corresponding planar motor and calculated by (1). If (1) is substituted into the right-hand sides of (3)-(4), we get a nonlinear dynamic model due to the exponential and sinusoidal spatial dependences in (1). Then, a DQ decomposition method is applied to the system as follows [16].

$$\begin{bmatrix} i_Q \\ i_D \end{bmatrix} = \begin{bmatrix} \cos\gamma_1 y & \sin\gamma_1 y \\ -\sin\gamma_1 y & \cos\gamma_1 y \end{bmatrix} \begin{bmatrix} \frac{2}{3} & -\frac{1}{3} & -\frac{1}{3} \\ 0 & \frac{1}{\sqrt{3}} & -\frac{1}{\sqrt{3}} \end{bmatrix} \begin{bmatrix} i_A \\ i_B \\ i_C \end{bmatrix} \tag{6}$$

Then, the force equation (1) can now be represented as follows.

$$\begin{bmatrix} f_y \\ f_z \end{bmatrix} = \frac{1}{2}\mu_0 M_0 \eta_0 N_m G e^{-\gamma_1 z_0} \begin{bmatrix} i_Q \\ i_D \end{bmatrix} \tag{7}$$

Since the travel range of the stage in the z-direction is less than 20 μm, compared to the air gap of 2.32 mm, displacement in the z-direction is very small. Thus the air gap z_0 can be regarded a constant value. After z_0 is fixed, the relations between f_y and i_Q and f_z and i_D are linear. As a result, the dynamics in the horizontal mode can be presented in the state-space form, which is shown as follows.

$$\begin{bmatrix} \dot{x} \\ \dot{y} \\ \dot{\varphi} \\ \dot{h} \\ \dot{u} \\ \dot{v} \end{bmatrix} = \begin{bmatrix} 0 & 0 & 0 & 1 & 0 & 0 \\ 0 & 0 & 0 & 0 & 1 & 0 \\ 0 & 0 & 0 & 0 & 0 & 1 \\ 0 & 0 & 0 & 0 & 0 & 0 \\ 0 & 0 & 0 & 0 & 0 & 0 \\ 0 & 0 & 0 & 0 & 0 & 0 \end{bmatrix} \begin{bmatrix} x \\ y \\ \varphi \\ h \\ u \\ v \end{bmatrix} + \begin{bmatrix} 0 & 0 & 0 \\ 0 & 0 & 0 \\ 0 & 0 & 0 \\ 0 & 0 & \frac{c}{m} \\ \frac{c}{m} & \frac{c}{m} & 0 \\ -\frac{c}{I_{zz}}l_{1y} & \frac{c}{I_{zz}}l_{2y} & 0 \end{bmatrix} \begin{bmatrix} i_{1q} \\ i_{2q} \\ i_{3q} \end{bmatrix}$$

$$y = \begin{bmatrix} 1 & 0 & 0 & 0 & 0 & 0 \\ 0 & 1 & 0 & 0 & 0 & 0 \\ 0 & 0 & 1 & 0 & 0 & 0 \\ 0 & 0 & 0 & 1 & 0 & 0 \\ 0 & 0 & 0 & 0 & 1 & 0 \\ 0 & 0 & 0 & 0 & 0 & 1 \end{bmatrix} \begin{bmatrix} x \\ y \\ \varphi \\ h \\ u \\ v \end{bmatrix} \tag{8}$$

In (8), x and y are displacements in the x- and y-directions respectively, and φ is the rotation about the z-axis. The currents, i_{1q}, i_{2q}, and i_{3q} are the quadrature currents in Motors I, II, and III, respectively, which make the stage move in the horizontal mode. The value of the force constant in (7) is 20.15 N/A. $I_{zz} = 0.054$ kg·m^2 is the moment of inertia about the z-axis. l_{1y} and l_{2y} are the lengths of the moment arms from the center of Motors I and II to the platen center of the mass, and their values are 49.745 mm and 52.719 mm, respectively. In our system, the output matrix is a 6 × 6 identity matrix. Because the laser interferometers can directly give the position and the velocity information to the controller, all the states in the horizontal dynamics are available.

In the vertical mode, because the stage is levitated by three aerostatic bearings, the system is modeled as a spring-mass-damper system as shown in Fig. 3. The three aerostatic bearings are modeled as three springs and dampers which have a spring constant of K_1, K_2, and K_3 and damping coefficients of C_1, C_2, and C_3, respectively. The three springs support the platen in parallel connection. Thus the dynamics of the stage in the vertical mode can be represented as follows.

$$M\frac{d^2z}{dt^2} = f - K_z z - Mg \tag{9}$$

$$I_{xx}\frac{d^2\theta}{dt^2} = \tau_\theta - K_\theta\theta - C_\theta\frac{d\theta}{dt} \tag{10}$$

$$I_{yy}\frac{d^2\psi}{dt^2} = \tau_\psi - K_\psi\psi - C_\psi\frac{d\psi}{dt} \tag{11}$$

By Hooke's law, the spring constant in the z-direction, K_z was experimentally determined to be 7.06×10^5 N/m. The torsional spring constants about the x and y-axes, K_θ and K_ψ were found to be 1.115×10^4 N·m/rad and 1.165×10^4 N·m/rad, respectively. The principal moments of inertia I_{xx} and I_{yy} about the x- and y-axes are 0.033 kg·m^2 and 0.025 kg·m^2,

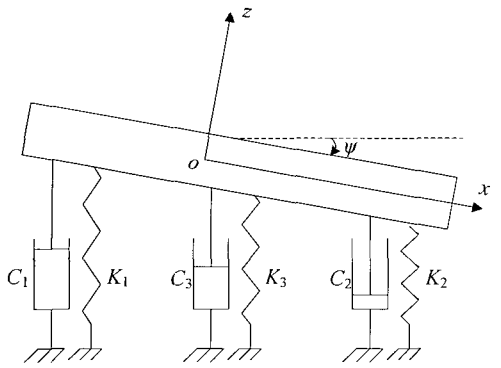

Fig. 3. Spring-mass-damper model in the vertical mode.

respectively. The damping coefficients C_θ and C_ψ are 2 N·m/rad/s. f_z is the vertical force and τ_θ, τ_ψ are the torques about the x- and y-axes generated by the planar motors. Using the linearized force equation (7), we derived the following state-space dynamic equation in the vertical mode:

$$\begin{bmatrix} \dot{z} \\ \dot{\theta} \\ \dot{\psi} \\ \dot{p} \\ \dot{q} \\ \dot{w} \end{bmatrix} = \begin{bmatrix} 0 & 0 & 0 & 1 & 0 & 0 \\ 0 & 0 & 0 & 0 & 1 & 0 \\ 0 & 0 & 0 & 0 & 0 & 1 \\ -\frac{K_z}{m} & 0 & 0 & 0 & 0 & 0 \\ 0 & -\frac{K_\theta}{I_{xx}} & 0 & 0 & -\frac{C_\theta}{I_{xx}} & 0 \\ 0 & 0 & -\frac{K_\psi}{I_{yy}} & 0 & 0 & -\frac{C_\psi}{I_{yy}} \end{bmatrix} \begin{bmatrix} z \\ \theta \\ \psi \\ p \\ q \\ w \end{bmatrix} + \begin{bmatrix} 0 & 0 & 0 \\ 0 & 0 & 0 \\ 0 & 0 & 0 \\ \frac{c}{m} & \frac{c}{m} & \frac{c}{m} \\ -\frac{c}{I_{xx}} l_{1y} & -\frac{c}{I_{xx}} l_{2y} & \frac{c}{I_{xx}} l_{3y} \\ \frac{c}{I_{yy}} l_{1x} & -\frac{c}{I_{yy}} l_{2x} & -\frac{c}{I_{yy}} l_{3x} \end{bmatrix} \begin{bmatrix} i_{1d} \\ i_{2d} \\ i_{3d} \end{bmatrix}$$

$$y = \begin{bmatrix} 1 & 0 & 0 & 0 & 0 & 0 \\ 0 & 1 & 0 & 0 & 0 & 0 \\ 0 & 0 & 1 & 0 & 0 & 0 \end{bmatrix} \begin{bmatrix} z \\ \theta \\ \psi \\ p \\ q \\ w \end{bmatrix}. \quad (12)$$

The constants l_{1y}, l_{2y}, l_{3y}, l_{1x}, l_{2x}, and l_{3x} in the input matrix are the lengths of the moment arms from the centers of the planar motors to the platen's mass center in the x- and y-directions. Their values are measured as l_{1x} = 49.7 mm, l_{2x} = 52.7 mm, l_{3x} = 1.3 mm, l_{1y} = 44.8 mm, l_{2y} = 44.8 mm, and l_{3y} = 84.3 mm. Unlike the laser interferometers in the horizontal mode, the laser distance sensors used in the vertical mode can only provide the displacement information. Thus, only the first three displacement states are measurable in the output matrix of (12).

It can be seen from the state-space dynamic equations of (8) and (12) that the system is modeled as a MIMO system. It has six current inputs i_{1q}, i_{2q}, i_{3q}, i_{1d}, i_{2d}, and i_{3d}, six displacement outputs x, y, φ, z, θ, and ψ, and three velocity outputs h, u, and v. Thus a multivariable control system design methodology can be applied to the system.

3. INTEGRATOR AUGMENTED LQ REGULATOR DESIGN

An LQ regulator inherently possesses good robustness properties. It guarantees a phase margin of at least 60° [17]. Furthermore, in an LQ design, some states can be intentionally penalized in the weighting matrix to achieve a desired dynamic performance. Therefore an LQR is suitable for the horizontal-mode control. However, there are two main drawbacks for an LQR to be used in a servo mechanism. One is that as a regulator, an original form of an LQR cannot track a non-zero reference input. The other is that there will be a steady-state error due to the nonexistence of integrators in an LQR. In order to make the LQR operational for our system, we need to derive the tracking-error dynamics of the system to design an integrator-augmented LQR. The errors are defined as follows.

$$\Delta \boldsymbol{x} = \boldsymbol{x} - \boldsymbol{x}^* \quad (13)$$

$$\Delta \boldsymbol{y} = \boldsymbol{y} - \boldsymbol{y}^* \quad (14)$$

$$\Delta \boldsymbol{u} = \boldsymbol{u} - \boldsymbol{u}^*, \quad (15)$$

where $\boldsymbol{x}$, $\boldsymbol{y}$, and $\boldsymbol{u}$ are the state, output, and input vectors of the state-space model in the horizontal mode, which is represented in (16), and $\boldsymbol{x}^*$, $\boldsymbol{y}^*$, and $\boldsymbol{u}^*$ are the corresponding steady-state vectors, respectively.

$$\begin{aligned} \dot{\boldsymbol{x}} &= A\boldsymbol{x} + B\boldsymbol{u} \\ \boldsymbol{y} &= C\boldsymbol{x} \end{aligned} \quad (16)$$

The A, B, and C are the corresponding state, input, and output matrices in (8), respectively. Taking the derivative of (13), we obtain the following error dynamics.

$$\Delta \dot{\boldsymbol{x}} = \dot{\boldsymbol{x}} - \dot{\boldsymbol{x}}^* = A(\boldsymbol{x} - \boldsymbol{x}^*) + B(\boldsymbol{u} - \boldsymbol{u}^*) = A\Delta \boldsymbol{x} + B\Delta \boldsymbol{u} \quad (17)$$

$$\Delta \boldsymbol{y} = C(\boldsymbol{x} - \boldsymbol{x}^*) = C\Delta \boldsymbol{x} \quad (18)$$

From (17)-(18), the model of the error dynamics is the same as that of the original dynamics. Next we augment integrators to the system to eliminate the steady-state error. Fig. 4 presents the structure of the integrator-augmented LQ controller.

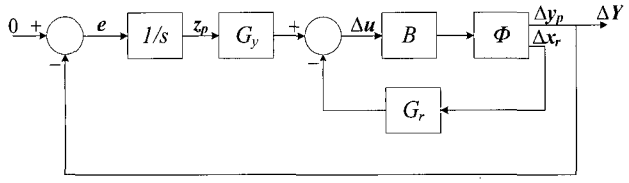

Fig. 4. Integrator-augmented LQ controller.

In Fig. 4, z_p is the integrator states and G_y and G_r are the LQ gain matrices for the integrator states and original states, respectively. The state-space model of the augmented system is presented as following.

$$\begin{bmatrix} \Delta\dot{\boldsymbol{x}}_p \\ \dot{\boldsymbol{z}}_p \end{bmatrix} = \begin{bmatrix} A_p & 0 \\ C_p & 0 \end{bmatrix} \begin{bmatrix} \Delta\boldsymbol{x}_p \\ \boldsymbol{z}_p \end{bmatrix} + \begin{bmatrix} B_p \\ 0 \end{bmatrix} \Delta\boldsymbol{u}_p \tag{19}$$

$$\Delta\boldsymbol{y}_p = \begin{bmatrix} C_p & 0 \end{bmatrix} \begin{bmatrix} \Delta\boldsymbol{x}_p \\ \boldsymbol{z}_p \end{bmatrix} \tag{20}$$

As a result, the augmented system now has nine states altogether in the horizontal mode. Since all the nine states are available, an LQR can be designed for the system based on the augmented system (19)-(20).

To eliminate the steady-state error effectively, we penalize the effect of the integrators heavily. The Q and R matrices are designed as follows.

$$Q = \text{diag}([10^4, 10^4, 10^5, 1, 1, 1, 10^8, 10^8, 10^{10}]) \tag{21}$$

$$R = I_{3\times 3} \tag{22}$$

The corresponding gain matrix K computed by Matlab is as follows.

$$K = \begin{bmatrix} 0 & 4089 & -10213 & 0 & 11.13 & -7.28 & 0 & 72696 & -68668 \\ 0 & 3859 & 10781 & 0 & 10.51 & 7.60 & 0 & 68668 & 72696 \\ 6280 & 0 & 0 & 19.22 & 0 & 0 & 10000 & 0 & 0 \end{bmatrix} \tag{23}$$

Thus the control law is

$$\boldsymbol{u} = -K\boldsymbol{X} + \boldsymbol{u}^*, \tag{24}$$

where $\boldsymbol{X}$ is the new 9-by-1 integrator-augmented state vector in (19), and $\boldsymbol{u}^*$ is the steady-state input vector to the system, which can be solved by plugging $\boldsymbol{x}^*$ into (8).

The closed-loop poles are placed at $-74.556 \pm 119.95i$, $-16.808 \pm 28.034i$, $-19.047 \pm 31.430i$, -135.60, -31.912, and -35.685. Closed-loop 10-μm and 10-μrad step responses are shown in Fig. 5. These step responses demonstrate a good tracking performance in the horizontal mode with short rise and settling times. Fig. 6 shows the error of these step responses in Fig. 5. From these plots, we can see that after 1 second the tracking errors in the x-, y-, and φ-axes are less than 0.15 μm, 0.08 μm, and 0.2 μrad, respectively. Thus the tracking errors in the horizontal

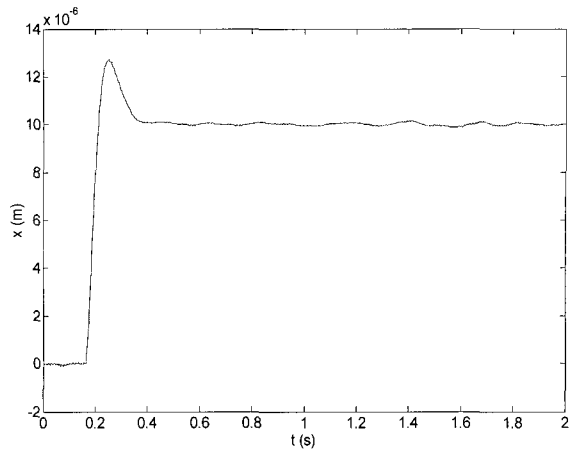

(a)

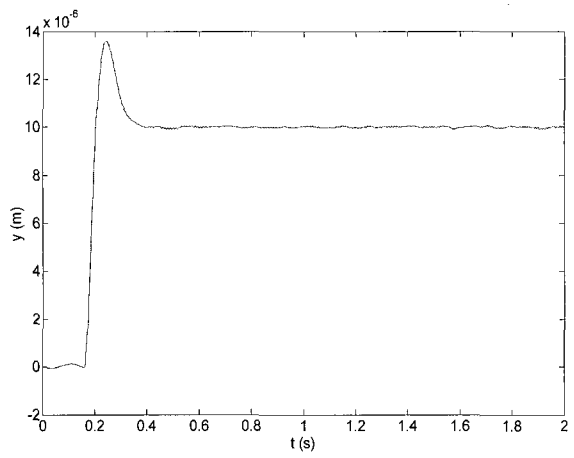

(b)

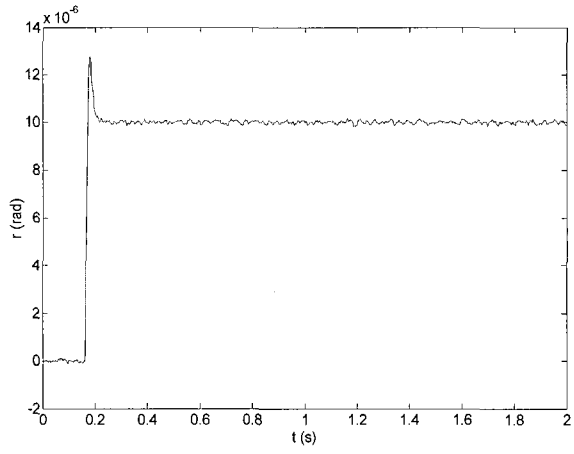

(c)

Fig. 5. Closed-loop 10-μm step responses in (a) x and (b) y. (c) Closed-loop 10-μrad step response in φ with the integrator-augmented LQ controller.

mode are less than 2% after 1 second. Key limiting factors in position resolution and tracking error include the acoustic noise generated by the aerostatic bearings and the disturbance transmitted through the umbilical cables attached to the moving platen.

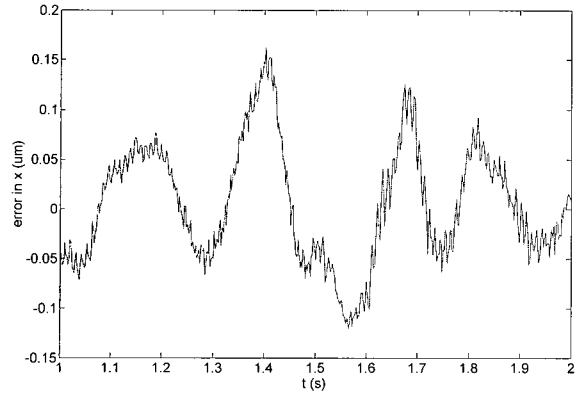

(a)

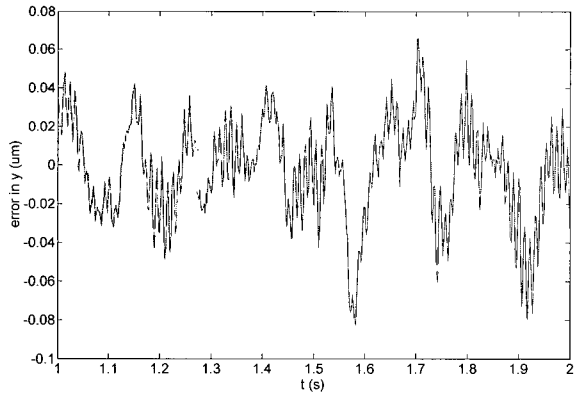

(b)

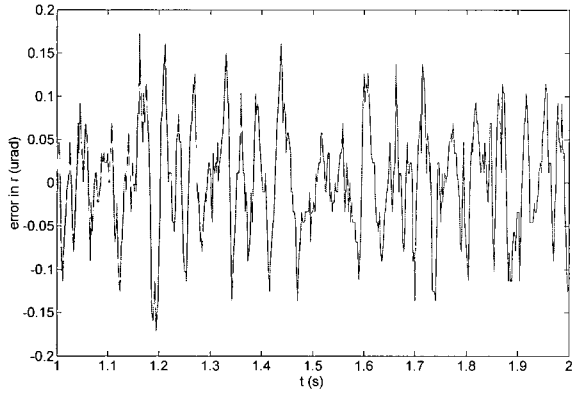

(c)

Fig. 6. Error in the 10-μm step responses in (a) x and (b) y. (c) Error in the 10-μrad step response in φ.

4. REDUCED-ORDER LQG CONTROLLER DESIGN

The LQR design in the previous section relies on the physical presence of the complete states. However, the laser distance sensor used in the vertical mode cannot directly provide the full states to the controller. In other words, some state variables (velocities) are not available to the controller. As a result, an observer is needed to reconstruct the unknown state variables. As well known, if (A, B) is stabilizable and (A, C) is detectable, it is possible to design an observer/state-feedback controller for the system. In our system both the above requirements are satisfied.

The LQG control methodology is the combination of a Kalman filter and an LQR control law [18]. Because the sensors in the vertical mode give the displacement measurements to the controller, it is unnecessary to implement a full-order observer. Instead, estimating only the unknown states makes the structure of controller more compact and saves much more computing time for the digital controller. Thus a reduced-order LQG controller is designed for the vertical mode. Similarly, in order to reduce the steady-state error, we need to use the integrator-augmented error-dynamics model which is similar to (19)-(20). Then the augmented system is divided into two subsystems in terms of the known state $\boldsymbol{x}_1$ and unknown state $\boldsymbol{x}_2$, which is shown in (25).

$$\begin{bmatrix}\dot{\boldsymbol{x}}_1\\ \dot{\boldsymbol{x}}_2\end{bmatrix}=\begin{bmatrix}A_{11} & A_{12}\\ A_{21} & A_{22}\end{bmatrix}\begin{bmatrix}\boldsymbol{x}_1\\ \boldsymbol{x}_2\end{bmatrix}+\begin{bmatrix}B_1\\ B_2\end{bmatrix}\boldsymbol{u}$$
$$\boldsymbol{y}=\begin{bmatrix}I & 0\end{bmatrix}\begin{bmatrix}\boldsymbol{x}_1\\ \boldsymbol{x}_2\end{bmatrix} \tag{25}$$

In (25), because the values of the measurable states can be obtained from the sensors, and the integrator states, by integration, these states can be treated as known states $\boldsymbol{x}_1$. On the other hand, the velocity states are regarded as unknown states $\boldsymbol{x}_2$. Then an estimator for $\boldsymbol{x}_2$ can be designed based on the methodology illustrated in [19]. The state matrix A and the input matrix B in (25) are also divided into sub-matrices according to the states $\boldsymbol{x}_1$ and $\boldsymbol{x}_2$, respectively. By matrix manipulations, the closed-loop dynamics of the reduced-order LQG control system can be derived as following.

$$\begin{bmatrix}\dot{\boldsymbol{x}}_1\\ \dot{\boldsymbol{x}}_2\\ \dot{\boldsymbol{b}}\end{bmatrix}=\begin{bmatrix}A_{11}-B_1k_1-B_1k_2L & A_{12} & -B_1k_2\\ A_{21}-B_2k_1-B_2k_2L & A_{22} & -B_2k_2\\ (A_{22}-LA_{12})L+A_{21}-LA_{11}-(B_2-LB_1)(k_1+k_2L) & 0 & A_{22}-LA_{12}-B_2k_2+LB_1k_2\end{bmatrix}\begin{bmatrix}\boldsymbol{x}_1\\ \boldsymbol{x}_2\\ \boldsymbol{b}\end{bmatrix} \tag{26}$$

where $\mathbf{b}=\hat{\mathbf{x}}_2-L\mathbf{x}_1$, and $\hat{\boldsymbol{x}}_2$ is the estimated state vector of $\boldsymbol{x}_2$. L is the estimator gain matrix. The LQ gain matrix K = [$\boldsymbol{k}_1$ $\boldsymbol{k}_2$] is divided into $\boldsymbol{k}_1$ for the known states and $\boldsymbol{k}_2$ for the estimated states. The LQ state-feedback control law for our system will be

$$\boldsymbol{u}=-(\boldsymbol{k}_1+\boldsymbol{k}_2L)\,\boldsymbol{x}_1-\boldsymbol{k}_2\boldsymbol{b}+\boldsymbol{u}^* \tag{27}$$
$$\boldsymbol{u}^*=-\mathrm{pinv}(B)A\boldsymbol{X}^*, \tag{28}$$

where pinv (B) is the pseudo-inverse of the B matrix in (25). $\boldsymbol{x}_1$ are the known displacement and integrator states given by the sensors and the integrators. From (26) the derivative of $\boldsymbol{b}$ is a function of $\boldsymbol{x}_1$ and $\boldsymbol{b}$, so the states $\boldsymbol{b}$ can be obtained by integrating the ordinary differential equations. $\boldsymbol{u}^*$ is calculated by (28), where the A and B matrices come from the state-space model in the vertical mode shown in (12). Therefore, the control law shown in (27) can be implemented, once

the gain matrix is determined. The closed-loop state matrix shown in (26) can be finally converted into the matrix shown in (29) by four-step matrix manipulations of the state matrix in (26):

a) column 3 × (−L) + column 1
b) row 1 × (L) + row 3
c) row 2 × (−1) + row 3
d) column 4 + column 3

$$\begin{bmatrix} A_{11}-B_1k_1 & A_{12}-B_1k_2 & -B_1k_2 \\ A_{21}-B_2k_1 & A_{22}-B_2k_2 & -B_2k_2 \\ 0 & 0 & A_{22}-LA_{12} \end{bmatrix} = \begin{bmatrix} A-BK & -Bk_2 \\ 0 & A_{22}-LA_{12} \end{bmatrix} \tag{29}$$

The matrix on the left hand side of (29) can be divided into four sub-matrices. Each of these sub-matrices is equal to the corresponding sub-matrix on the right hand side of (29). The separation principle is used in the design of a reduced order LQG controller. If (A, B) is stabilizable and (A_{22}, A_{12}) is detectable, the state-feedback gain matrix K and the Kalman-filter gain matrix L can be determined by the LQR and Kalman-filter design methodologies, respectively. Both (A, B) and (A_{22}, A_{12}) meet the requirements for the design. The LQ controller is first designed as follows.

$$Q = \text{diag}([10^4\ 10^3\ 10^3\ 10^{10}\ 10^9\ 10^9\ 10^2\ 10^2\ 10^2])$$
$$R = \begin{bmatrix} 1 & 0 & 0 \\ 0 & 1 & 0 \\ 0 & 0 & 1 \end{bmatrix} \tag{30}$$

$$K = \begin{bmatrix} -7524 & 2870 & -10989 & 57884 & -13274 & 67240 & 6.09 & -1.37 & 3.15 \\ -10948 & 3568 & 9790 & 55164 & -12709 & -70356 & 6.01 & -1.33 & -3.30 \\ -4642 & -7296 & 3.77 & 59010 & 24929 & -11777 & 6.16 & 2.55 & -0.02 \end{bmatrix} \tag{31}$$

For the Kalman-filter design, the measurement and process noises existing in the system are considered as stationary zero-mean white Gaussian noises. Thus the plant model can be represented as follows.

$$\begin{aligned} \dot{\boldsymbol{x}}(t) &= A\boldsymbol{x}(t) + Bu(t) + H\zeta(t) \\ \boldsymbol{y}(t) &= C\boldsymbol{x}(t) + \theta(t), \end{aligned} \tag{32}$$

where the A, B, H, and C are constant matrices, and $\zeta(t)$ and $\theta(t)$ are process and measurement noises, respectively. They have the following properties.

$$E\{\zeta(t)\} = 0 \tag{33}$$
$$\text{cov}\{\zeta(t), \zeta(t)\} = \Psi\delta(t-\tau),\ \Psi = \Psi^T \tag{34}$$
$$E\{\theta(t)\} = 0 \tag{35}$$
$$\text{cov}\{\theta(t), \theta(t)\} = \Theta\delta(t-\tau),\ \Theta = \Theta^T, \tag{36}$$

where $E\{\cdot\}$ is the expectation operator and $\delta(t-\tau)$ is a dalta function. Therefore, the kalman gain matrix L can be determined by solving a filter algebraic Ricatti equation (FARE), which is presented as following

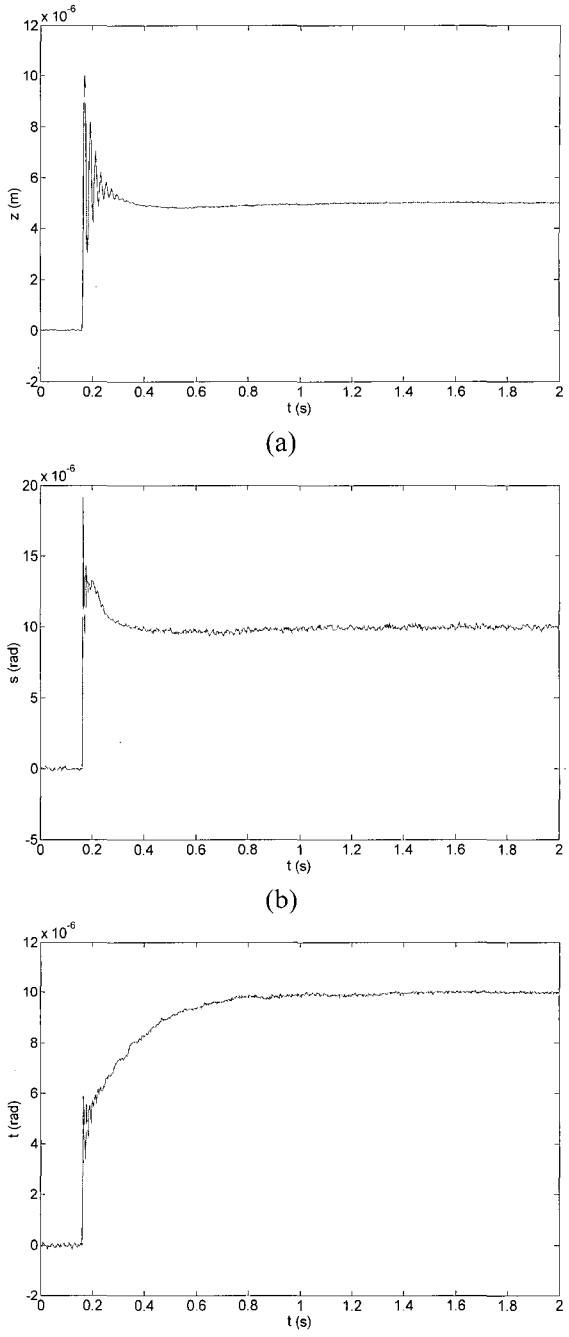

Fig. 7. (a) Closed-loop 5-μm step response in z, and 10-μrad step responses in (b) θ and (c) ψ with the reduced-order integrator-augmented LQG controller.

$$A\Sigma + \Sigma A^T + H\Psi H^T - \Sigma C^T\Theta^{-1}C\Sigma = 0, \tag{37}$$
$$L = \Sigma C^T\Theta^{-1}. \tag{38}$$

Using the Matlab command "kalman," we calculated the gain matrix L as follows.

$$L = \begin{bmatrix} 9977 & 0 & 0 & 0.998 & 0 & 0 \\ 0 & 9955 & 0 & 0 & 0.997 & 0 \\ 0 & 0 & 9938 & 0 & 0 & 0.995 \end{bmatrix} \tag{39}$$

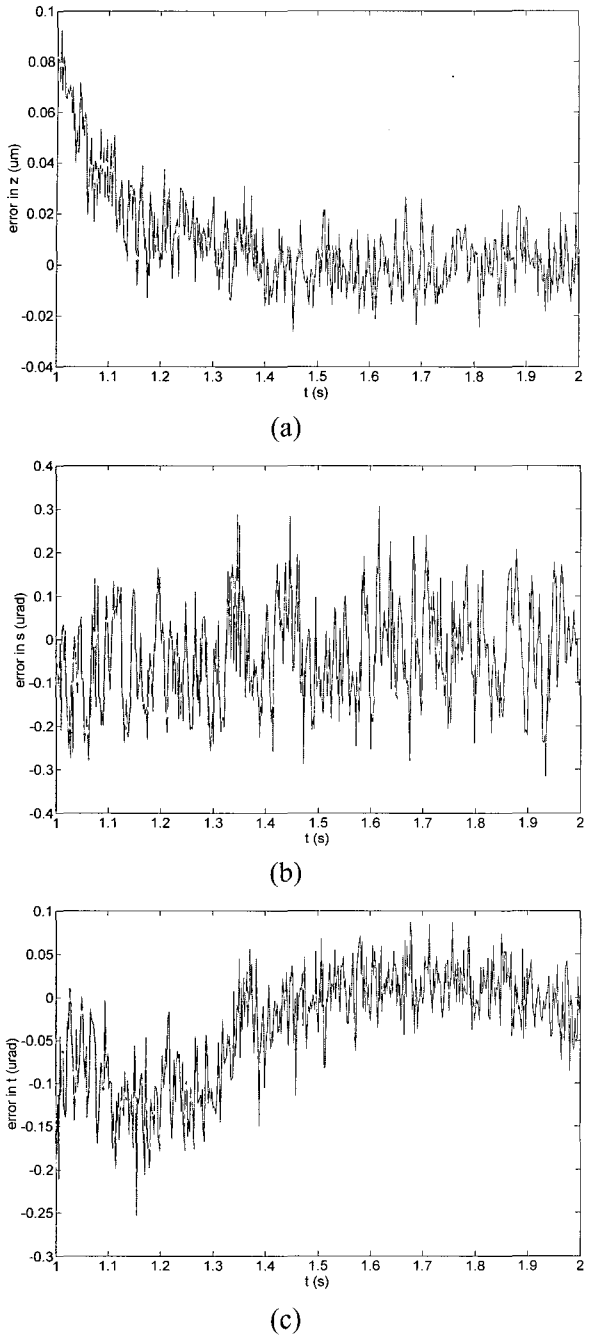

Fig. 8. Errors in (a) 5-μm step response in z and in 10-μrad step responses in (b) θ and (c) ψ.

After implementing this reduced-order integrator-augmented LQG controller, we obtained closed-loop step responses in the vertical mode shown in Fig. 7.

Fig. 8 presents the steady-state errors of the step responses in Fig. 7. These plots show that after 1 second the tracking error in the z-axis is less than 0.08 μm and those in the θ- and ψ-axes are less than 0.3 μrad, respectively. Thus the steady-state errors in the vertical mode are all less than 3%, which indicates the reduced-order integrator augmented LQG controller successfully controlled the system in the vertical mode. However, in the vertical mode, the errors are a little bigger than those in the horizontal mode because the laser distance sensors used in the vertical mode have lower resolution and larger electronic noise compared to the laser interferometers in the horizontal mode. Furthermore, the acoustic noises from the three aerostatic bearings for levitation are the other main error sources.

5. CONCLUSIONS

In this paper, we presented the modeling and multivariable feedback controller design for a novel integrated multidimensional positioning stage. This novel stage has only a 5.91-kg single moving part and is based on a patented concentrated-field magnet matrix. The system was modeled as a MIMO system. The dynamics of the system was studied in the horizontal and vertical modes. Two state-space models (in the horizontal and vertical modes, respectively) were developed for the system.

The detailed process of designing multivariable controllers for the positioning stage was presented in this paper. An integrator-augmented LQR was first designed and implemented in the horizontal mode. The step responses and error-analysis results demonstrated the integrator-augmented LQ controller's good tracking performance and high-resolution positioning capabilities.

Since the sensors in the vertical mode cannot measure the velocity states, an LQG controller was designed in the vertical mode. To reduce the computation time for the digital controller, a reduced-order LQG controller with integrators was implemented. The experimental results in the vertical mode demonstrated the effectiveness of this multivariable controller.

REFERENCES

[1] F. Schellenberg, "A little light magic [Optical lithography]," *IEEE Spectrum*, vol. 40, no. 9, pp. 34-39, September 2003.

[2] Semiconductor Industry Association 2004 Annual Report, pp. 50, 2004.

[3] R. A. de Callafon and P. M. J. Van den Hof, "Multivariable feedback relevant system identification of a wafer stepper system," *IEEE Trans. on Control System Technology*, vol. 9, no. 2, pp. 381-382, March 2001.

[4] Z. Z. Liu, F. L. Luo, and M. H. Rashid, "Robust high speed and high precision linear motor direct-drive xy-table motion system," *Proc. of IEE Control Theory and Applications*, vol. 151, no. 2, pp. 166-173, March 2004.

[5] S. Salapaka and A. Sebastian, "Design of high precision high bandwidth and reliable nanopositioning systems," *Proc. of IMECE'03*, IMECE2003-55554, November 2003.

[6] M. Kobayashi and R. Horowitz, "Track seek control for hard disk dual-stage servo systems," *IEEE Trans. on Magnetics*, vol. 37, no. 2, pp. 949-954, March 2001.

[7] Piezo Systems, Inc, "Introductions to Piezo Transducers," http://Piezo Systems - piezo actuators & transducers.htm, 2005.

[8] J. Cao, Y. Zhu, J. Wang, W. Yin, and G. Duan, "Analysis and comparison of two-dimensional permanent-magnet arrays for planar motor," *IEEE Trans. on Magnetics*, vol. 40, no. 6, pp. 3490-3494, November 2004.

[9] H.-S. Cho, C.-H. Im, and H.-K. Jung, "Magnetic field analysis of 2-D permanent magnet array for planar motor," *IEEE Trans. on Magnetics*, vol. 37, no. 5, pp. 3762-3766, September 2001.

[10] J. Pan, N. C. Cheung, and J. Yang, "Structure and characteristics of closed-loop two-dimensional surface motors-A literature survey," *Proc. of IEEE the 5th International Conference on Power Electronics and Drive Systems*, pp. 236-241, November 2003.

[11] D. L. Trumper, W.-J. Kim, and M. E. Williams, "Magnetic Arrays," US Patent 5 631 618, May 1997.

[12] W.-J. Kim, *High-Precision Planar Magnetic Levitation*, Doctoral Thesis, Massachusetts Institute of Technology, June 1997.

[13] W.-J. Kim, N. Bhat, and T. Hu, "Integrated multidimensional positioner for precision manufacturing," *Journal of Engineering Manufacture: Proceedings of the Institution of Mechanical Engineers, Part B*, vol. 218, no. 4, pp. 431-442, April 2004.

[14] D. de Roover, *Motion Control of a Wafer Stage; A Design Approach for Speeding Up IC Production*, Doctoral Thesis, Delft Universtiy Technology, Delft, The Netherlands, 1997.

[15] D. L. Trumper, W.-J. Kim, and M. E. Williams, "Design and analysis framework for permanent-magnet machines," *IEEE Trans. on Industry Applications*, vol. 32, no. 2, pp. 371-379, March/April 1996.

[16] M. Konghirun and L. Xu, "A DQ-axis current control technique for fast transient response in vector controlled drive of permanent magnent synchronous motor," *Proc. of IEEE Power Electronics and Motion Control Conference*, pp. 1316-1320, August 2004.

[17] C. Zhang and M. Fu, "A revisit to the gain and phase margins of linear quadratic regulators," *IEEE Trans. on Automatic Control*, vol. 41, no. 10, pp. 1527-1530, October 1996.

[18] S. Skogestad and L. Postlethwaite, *Multivariable Feedback Control Analysis and Design*, John Wiley & Sons, New York, NY, 1996.

[19] J. S. Bay, *Fundamentals of Linear State Space Systems*, WCB/McGraw-Hill, Boston, MA, 1999

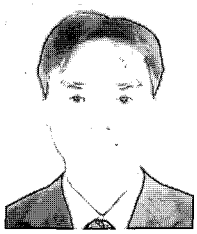

Tiejun Hu received the B.S. degree in Mechanical Engineering and the M.S. degree in Material Processing Engineering from Tsinghua University, Beijing, China, in 1999 and 2002, respectively, and the Ph.D. degree in Mechanical Engineering from Texas A&M University, College Station, in May 2005. His doctoral dissertation project involved design and control of a novel 6-degree-of-freedom (DOF) levitated stage with high precision. The integrated multi-dimensional positioning stage can be used in precision manufacturing and has the potential to satisfy the requirements for next generation wafer FABs in semiconductor manufacturing. Dr. Hu was a Research Assistant at Precision Mechatronics and Nanotechnology Lab, Department of Mechanical Engineering at Texas A&M University, College Station. His research interests are control system design, high precision servo mechanism design, embedded system design and development, nanoscale engineering and technology, power electronics, and digital signal processing. Dr. Hu is a student member of ASME.

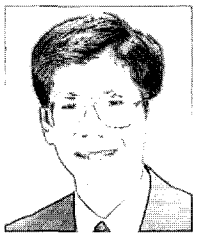

Won-jong Kim received the B.S. (summa cum laude) and M.S. degrees in Control and Instrumentation Engineering from Seoul National University, Seoul, Korea, in 1989 and 1991, respectively, and the Ph.D. degree in Electrical Engineering and Computer Science from Massachusetts Institute of Technology (MIT), Cambridge, in 1997. In September 2000, he joined the Department of Mechanical Engineering, Texas A&M University (TAMU), College Station, where he is currently an Assistant Professor. Following receipt of the Ph.D. degree, he was with SatCon Technology Corporation, Cambridge, MA, for three years. His teaching and research interests focus on analysis, design, and real-time control of mechatronic systems, networked control systems, and nanoscale engineering and technology. He holds three US patents on precision positioning systems. Dr. Kim received the Grand Prize from the Korean Institute of Electrical Engineers' Student Paper Contest in 1988. His 1997 MIT dissertation earned him the Gold Prize from Samsung Electronics' Humantech Thesis Prize. He was a semifinalist of the NIST's Advanced Technology Program 2000 Competition. The NASA granted him the Space Act Award in 2002. He was appointed a Select Young Faculty Fellow by TAMU College of Engineering and the Texas Engineering Experiment Station twice in 2003 and 2005. He received the PE Publishing Award for the best paper published in the 2004 volume of Journal of Engineering Manufacture in 2005. He is the Chair of the ASME Nanoscale Control Technical Panel and a member of the IEEE Nanotechnology Council. Prof. Kim is a Senior Member of IEEE and a Member of ASME, ASPE, KSEA, Pi Tau Sigma, and Sigma Xi.